

Unsteady Aerodynamics of an Oscillating Cascade in a Compressible Flow Field

Daniel H. Buffum and Donald R. Boldman
Lewis Research Center
Cleveland, Ohio

and

Sanford Fleeter
Purdue University
West Lafayette, Indiana

Prepared for the
4th Symposium on Unsteady Aerodynamics and Aeroelasticity of
Turbomachines and Propellers
sponsored by Aachen University of Technology
Aachen, West Germany, September 6-10, 1987



{NASA-TM-100219} UNSTEADY AERODYNAMICS OF
AN OSCILLATING CASCADE IN A COMPRESSIBLE
FLOW FIELD (NASA) 22 p Avail: NTIS HC
A03/MF A01 CSCL 20E

N88-13346

Unclas
G3/07 0114103

ERRATA

NASA Technical Memorandum 100219

UNSTEADY AERODYNAMICS OF AN OSCILLATING
CASCADE IN A COMPRESSIBLE FLOW FIELD

Daniel H. Buffum, Donald R. Boldman, and Sanford Fleeter
September 1987

Page 16, figure 10:

(A) Free-stream Mach number,
M, 0.65; mean flow incidence
angle, α_0 , 0° ; and reduced
frequency, k, 0.557

(B) Free-stream Mach number,
M, 0.80; mean flow
incidence angle, α_0 , 7° ;
and reduced frequency, k,
0.462.

Figure 10. - Effect of interblade phase angle on dynamic pressure
difference coefficient.

Page 19, figure 14(B): A square should appear at $-1.25 \times -90^\circ$.

UNSTEADY AERODYNAMICS OF AN OSCILLATING CASCADE
IN A COMPRESSIBLE FLOW FIELD

Daniel H. Buffum and Donald R. Boldman
National Aeronautics and Space Administration
Lewis Research Center
Cleveland, Ohio 44135

Sanford Fleeter
Thermal Sciences and Propulsion Center
School of Mechanical Engineering
Purdue University
West Lafayette, Indiana 47907

SUMMARY

Fundamental experiments were performed in the NASA Lewis Transonic Oscillating Cascade Facility to investigate and quantify the unsteady aerodynamics of a cascade of biconvex airfoils executing torsion-mode oscillations at realistic reduced frequencies. Flush-mounted, high-response miniature pressure transducers were used to measure the unsteady airfoil surface pressures. The pressures were measured for three interblade phase angles at two inlet Mach numbers, 0.65 and 0.80, and two incidence angles, 0° and 7°. The time-variant pressures were analyzed by means of discrete Fourier transform techniques, and these unique data were then compared with predictions from a linearized unsteady cascade model. The experimental results indicate that the interblade phase angle had a major effect on the chordwise distributions of the airfoil surface unsteady pressure, and that reduced frequency, incidence angle, and Mach number had a somewhat less significant effect.

SYMBOLS

C airfoil chord
 C_M unsteady moment coefficient about midchord,

$$\int_0^1 \left(\frac{1}{2} - \frac{x}{C} \right) \Delta C_p d\left(\frac{x}{C} \right)$$

C_p unsteady pressure coefficient, $p_1 / \frac{1}{2} \rho V^2 \bar{\alpha}$
 C_{p1} lower surface unsteady pressure coefficient
 C_{pu} upper surface unsteady pressure coefficient
 ΔC_p $C_{p1} - C_{pu}$
f oscillation frequency, Hertz or cycles/sec

k	reduced frequency, $\omega C/2V$
M	free-stream Mach number
p	time-variant static pressure
p_1	first harmonic of unsteady static pressure
S	airfoil spacing
t	time
V	free-stream velocity
x	chordwise coordinate
α_0	mean flow incidence angle
$\bar{\alpha}$	torsional oscillation amplitude
γ	stagger angle
ρ	free-stream density
σ	interblade phase angle (positive when airfoil n leads airfoil $n + 1$)
τ	maximum airfoil thickness
φ	phase lead relative to airfoil motion
ω	oscillation frequency, radians/sec

INTRODUCTION

In the rotating blade rows of turbomachines and turboprops, the severe flow conditions associated with off-design, positive-incidence operation cause continual concern about the possibility of flutter. Flutter prediction and, in particular, the modeling of nonzero-incidence-angle, unsteady cascade aerodynamics, have not kept pace with the overall advances and new requirements of turbomachine and turboprop designs. As a result, current semi-empirical flutter design systems are often unreliable.

The development of analyses to predict oscillating cascade aerodynamics is an item of fundamental research interest at both zero and nonzero incidence angles. Classical unsteady aerodynamic models are based on linearized theory, with the unsteady flow assumed to be a small perturbation of a uniform steady flow. The problem is reduced simply to analyzing the unsteady aerodynamics of a cascade of flat plates operating at zero mean incidence (refs. 1 and 2). As a result, the unsteady aerodynamics effects that are caused by the interaction between the steady and unsteady flow fields (i.e., the effects of blade geometry and nonzero incidence angle, or steady loading) are not considered. To overcome these limitations, models are being developed (refs. 3 to 8) in which the unsteady flow is coupled to a nonuniform steady flow field.

Data from oscillating cascade experiments are needed, particularly in the high subsonic and transonic flow regimes, in order to direct the development and evaluation of advanced unsteady aerodynamic models as well as to evaluate existing analyses. These flow regimes, however, are relatively unexplored. Unsteady pressure data have been obtained in a transonic linear cascade in which only the instrumented airfoil was forced to oscillate harmonically (ref. 9). In the subsonic compressible through supersonic flow regimes, an annular cascade has been used to obtain unsteady moment data from strain gages (ref. 10). Unsteady pressure measurements have been made at the NASA Lewis Research Center on a biconvex airfoil in a transonic oscillating cascade (ref. 11). Some anomalies exist in these unsteady data as well as in the steady airfoil-surface static pressure data. These are associated with (1) failure to maintain the profile of the airfoil instrumented with static pressure taps, (2) an unreliable airfoil motion signal, and (3) the misinterpretation of the schlieren flow visualization.

The NASA Lewis Transonic Oscillating Cascade Facility was used to investigate and quantify the unsteady aerodynamics of a cascade of biconvex airfoils executing torsion-mode oscillations at realistic reduced frequencies. Unsteady data analysis anomalies were eliminated and additional new unsteady aerodynamic data were analyzed. In particular, flush-mounted, high-response miniature pressure transducers were used to measure the unsteady airfoil surface pressures for three interblade phase angles at inlet Mach numbers of 0.65 and 0.80 and incidence angles of 0° and 7°. The time-variant pressures on the surfaces of the oscillating cascaded airfoils were then analyzed with discrete Fourier transform techniques.

OSCILLATING CASCADE FACILITY

The NASA Lewis Transonic Oscillating Cascade Facility (fig. 1) is a linear cascade wind tunnel capable of test section Mach numbers approaching unity. Air drawn from the atmosphere passes through a smoothly contracting inlet section into a constant-area 9.78- by 19.21-cm test section and then through a diffuser and exhaust header that has a nominal pressure of 3.0 N/cm². The flow rate is controlled by two valves located in the header. Upstream of the test section, a partitioned bleed system removes the boundary layers on each end wall and also establishes the steady airfoil passage-to-passage periodicity. The boundary layers on the upper and lower cascade walls are removed through tailboard slots.

A major feature of this facility is the high-speed mechanical drive system that imparts controlled torsional harmonic oscillations to the nine cascaded airfoils. Nine barrel cams, each with a six-cycle sinusoidal groove machined into its periphery, are mounted on a common shaft driven by a 74.6-kW electric motor. Connecting arms, joined to one end of each airfoil by trunnions, have buttons on the opposite end to follow the cam grooves. The amplitude of the sinusoidal airfoil motion, dictated by the cam and follower geometry, is 1.2°. Different interblade phase angle oscillations are achieved by changing the relative positions of the cams. In this investigation, the maximum oscillation frequency was 500 Hz, corresponding to a reduced frequency of 0.462 with a cascade inlet Mach number of 0.80.

AIRFOILS AND INSTRUMENTATIONS

The cascade comprised nine uncambered biconvex airfoils with a chord of 7.62 cm, a thickness-to-chord ratio of 0.076, a solidity of 1.3, and a stagger angle of 53° (fig. 2). The radius of curvature of the airfoil surfaces was 27.4 cm and the leading and trailing edges were rounded with a 0.025-cm radius of curvature. The airfoils were supported by two midchord trunnions, giving an elastic axis location at midchord.

The primary data quantified the complex unsteady surface pressures on the oscillating cascaded airfoils. These data were obtained by flush-mounting six miniature dynamic pressure transducers symmetrically along the chord of one airfoil surface (table I). Thus, to obtain the unsteady pressure data on both airfoil surfaces, the experiments were performed in two phases, with data acquired on one surface at a time. The transducers, each with an active sensor diameter of 0.0097 cm (1.3 percent of the airfoil chord), were placed in milled slots and potted in RTV (room-temperature vulcanizing) to isolate them from airfoil strain.

The time-variant position of the oscillating instrumented airfoil was determined by two independent measurements. The results of reference 11 were derived by using an electro-optical displacement meter to track the motion of the instrumented center airfoil. The second measure of the airfoil motion was provided by a proximity sensor that produces a voltage proportional to the air gap between it and an adjacent object. This sensor was positioned to face a six-cycle, sinusoidally shaped cam mounted on the same shaft as the airfoil drive cams and to be in phase with the instrumented airfoil motion. Samples of these two signals are shown in figure 3. The proximity probe signals were virtually noise free, although they appeared to be slightly nonsinusoidal near the positive signal peaks. Noise in the optical signals was a major concern. The noise was sometimes of so much greater intensity than shown in this figure that there was no discernible sinusoid.

The two signals were generally in good agreement, with a difference of 5 deg or less in the phase measurement of the airfoil motion. Under such conditions, either signal can be used as a reference for the unsteady pressure measurements. In some cases, however, there were large phase differences between the two measurements. These differences were most likely caused by the excessive noise in the optical signal or by the dropout of that signal altogether. The proximity probe signals were used to measure the airfoil motion in these experiments because of their high reliability.

DATA ACQUISITION AND ANALYSIS

All of the unsteady signals were ac-coupled and recorded on magnetic tape for postexperiment processing. During tape playback, the signals were simultaneously digitized at rates sufficient to capture at least three harmonics of the oscillation frequency; 32 768 samples were taken per channel. Each data channel was divided into blocks, typically with 2048 samples in each block, and then Fourier decomposed and referenced to the airfoil motion by subtracting the phase of the motion signal from the pressure signal. When all of the transducer signal blocks were decomposed, the results were averaged and data points with wideband noise spectra were discarded. To minimize errors caused

by spectral leakage, a correction scheme was applied to the decomposed results in conjunction with a Hanning window (ref. 12).

To demonstrate this data analysis technique, the pressure transducer signals shown in figure 4 were considered. The resulting averaged pressure spectra are presented in figure 5. The small spikes at 60 and 120 Hz were caused by noise picked up during signal transmission. The lack of any broad-band components indicates that the noise in the pressure signals was removed by the averaging process.

The final unsteady pressure data were in the form of a complex dynamic pressure difference coefficient ΔC_p (the difference between the lower surface and upper surface unsteady pressure coefficients) that defines the nondimensional pressure difference across the chordline of an airfoil. These data are presented in the format of a magnitude and a phase referenced to the airfoil motion, with the positive phase corresponding to the unsteady pressure that leads the airfoil motion.

RESULTS

A series of experiments was performed to investigate and quantify the effects of inlet Mach number, reduced frequency, interblade phase angle, and mean flow incidence angle on the unsteady aerodynamics of the oscillating cascade. The experimental conditions are summarized in table II. The airfoil motion is defined as

$$\alpha(t) = \alpha_0 + \bar{\alpha} \cos \omega t \quad (1)$$

where the oscillation amplitude $\bar{\alpha}$ is 1.2° and α_0 is the mean flow incidence angle.

The interblade phase angles at which acoustic resonances may occur can be predicted from linearized unsteady aerodynamic theory. The resonance conditions for the cascade geometry and flow conditions are defined in table III. Note that the experiments included both subresonant and superresonant conditions, with several data sets obtained in the immediate vicinity of an acoustic resonance.

Mach Number

Data were obtained at two values of the cascade inlet Mach number. At a Mach number of 0.65, the flow field was compressible and shock free. At the higher Mach number of 0.80, a shock was present in the flow field, confirmed by schlieren images of the oscillating leading-edge shock (ref. 11). Figure 6 presents the dynamic pressure difference coefficient data at 7° of incidence, 0° interblade phase angle, and oscillation frequencies of 200 and 500 Hz. The phase data show minimal variations with Mach number. At the lower frequency, the Mach number had little effect on the magnitude data. At the higher frequency, however, the Mach number had a large effect, with the largest pressure levels being associated with the lowest Mach number data.

Reduced Frequency

Reduced frequency significantly affected the phase of the dynamic pressure coefficient data only at a 0° interblade phase angle. This is demonstrated for interblade phase angles of -90° , 90° , and 0° in figure 7. The magnitude generally increased as the reduced frequency increased for interblade phase angles of -90° and 90° , with the lowest-reduced-frequency data having the smallest magnitudes. Unsteady data with wideband noise pressure spectra were discarded.

Mean Flow Incidence Angle

At the lower Mach number of 0.65, data were obtained and analyzed at both 0° and 7° of incidence. The dynamic pressure difference coefficient phase data were dependent on the mean flow incidence angle only at an interblade phase angle of 0° (fig. 8). This result is analogous to that previously noted for reduced frequency. As the incidence angle increased, the dynamic pressure difference coefficient magnitude data generally increased in value near the leading edge, but decreased with increasing chord.

Time histories of the unsteady pressure signals were investigated for evidence of flow separation. Carta and Lorber (ref. 13) found that flow separation is characterized by an abrupt change in the pressure level and is accompanied by an increase in the level of high-frequency pressure fluctuations. The pressure histories of the 12-, 25-, and 40-percent-chord transducer signals are shown in figure 9 for an inlet Mach number of 0.65. At 0° of incidence (fig. 9(a)), the pressure signals were sinusoidal with disturbances superimposed. Because separation is unlikely at 0° of incidence, the disturbances are representative of nonseparated flow fluctuations. At 7° of incidence (fig. 9(b)), the 12-percent-chord pressure signal showed increased-magnitude, high-frequency fluctuations near the pressure minimums. There was no indication of massive flow separation, however.

Figure 4 presents the pressure signals at Mach 0.80 and 7° of incidence. Although there were large random fluctuations, the precipitous pressure change indicative of flow separation was not present. For these flow conditions, reference 11 concludes that massive separation from the airfoil leading edge occurs as the airfoil pitches upward toward maximum incidence angle. This conclusion is based on schlieren motion pictures, which clearly show a region cyclically forming on the upper surface of the airfoils. Because the unsteady pressure data showed no evidence of massive flow separation (including the correlation of these data with an attached-flow prediction to be presented later), there is reason to believe that the flow visualization was misinterpreted, with the gradient in the schlieren motion pictures being most likely a slip line emanating from the leading-edge shock.

Interblade Phase Angle

Figure 10 shows the effect of interblade phase angle on the dynamic pressure difference coefficient for inlet Mach numbers of 0.65 and 0.80. For both 90° and -90° interblade phase angles, the magnitude data had approximately equal amplitudes near the leading edge, and decreased with increasing chordwise position. For a 0° interblade phase angle, however, the magnitude data

decreased relative to the nonzero interblade phase angle data, with no leading-edge maximums evident. Also, the phase data increased linearly with increasing chordwise position.

Data-Linearized Theory Correlation

The dynamic pressure coefficient data obtained in these experiments were compared with predictions from the unsteady, small-perturbation, subsonic, flat-plate cascade analyses of references 1 and 2. Figure 11 presents the results at reduced frequencies of 0.223 and 0.557 for an inlet Mach number of 0.65 and a mean incidence angle of 0° . The phase-lead data and predictions exhibited general agreement; the magnitude correlation quality varied with reduced frequency and interblade phase angle. Increasing the mean flow incidence angle to 7° while still maintaining the reduced frequency and Mach number values had a favorable effect on the correlation of the phase angle data and also, for the most part, of the magnitude data (fig. 12). Increasing the inlet Mach number to 0.80 while maintaining the incidence angle at 7° resulted in reduced frequencies of 0.185 and 0.462. As shown in figure 13, there was generally good correlation of the phase angle data at both reduced frequencies, and excellent correlation of the magnitude data at a reduced frequency of 0.185. The correlation was not as good, however, at a reduced frequency of 0.462.

The torsion-mode unsteady aerodynamic moment coefficients C_M were calculated from the unsteady pressure difference coefficient data. This was accomplished by (1) assuming a zero pressure difference at the leading and trailing edges of the airfoil, (2) fitting a smooth curve through the chordwise distribution of the data, and (3) numerically integrating the resulting chordwise distribution of the pressure difference.

The imaginary part of these experimentally determined moment coefficients, together with the corresponding predictions, are presented as a function of the interblade phase angle in figures 14 and 15. The data and predictions exhibited the same trends as the interblade phase angle increased from -90° toward 90° . At an interblade phase angle of 90° , however, a flutter instability was indicated by some of the data. The corresponding predictions were consistently lower in value, implying a more stable condition (i.e., the predictions were not conservative).

SUMMARY OF RESULTS

Fundamental experiments were performed in the NASA Lewis Transonic Oscillating Cascade Facility to investigate and quantify the unsteady aerodynamics of a cascade of biconvex airfoils executing torsion-mode oscillations at realistic reduced frequencies ranging from 0.185 to 0.557 in a compressible flow field. Flush-mounted, high-response pressure transducers were used to measure the unsteady airfoil surface pressures for several interblade phase angles at inlet Mach numbers of 0.65 and 0.80 and incidence angles of 0° and 7° .

The analysis of these unique data showed that the interblade phase angle had a major effect on the chordwise distributions of the airfoil surface unsteady pressure, with the effects of reduced frequency, incidence angle, and Mach number being somewhat less significant. Also, both the unsteady pressure

difference and the imaginary moment coefficient data generally correlated well with predictions from a linearized cascade model. However, at an interblade phase angle of 90° , where the data indicated a flutter instability, the corresponding predictions were consistently lower, implying a more stable condition (i.e., the predictions were not conservative).

REFERENCES

1. Smith, S.N.: Discrete Frequency Sound Generation in Axial Flow Turbomachines. ARC-R/M-3709, 1971.
2. Fleeter, S.: Fluctuating Lift and Moment Coefficients for Cascaded Airfoils in a Nonuniform Compressible Flow. J. Aircr., vol. 10, no. 2, Feb. 1973, pp. 93-98.
3. Atassi, H.; and Akai, T.J.: Aerodynamic and Aeroelastic Characteristics of Oscillating Loaded Cascades at Low Mach Number. ASME Paper 79-GT-111, Mar. 1979.
4. Verdon, J.M.; and Caspar, J.R.: Subsonic Flow Past an Oscillating Cascade with Finite Mean Flow Deflection. AIAA J., vol. 18, no. 5, May 1980, pp. 540-548.
5. Verdon, J.M.; and Caspar, J.R.: A Linearized Unsteady Aerodynamic Analysis for Transonic Cascades. J. Fluid Mech., vol. 149, Dec. 1984, pp. 403-429.
6. Whitehead, D.S.; and Grant, R.J.: Force and Moment Coefficients for High Deflection Cascades. Aeroelasticity in Turbomachines, P. Suter, ed., Juris-Verlag, 1980, pp. 85-127.
7. Chiang, H.D.; and Fleeter, S.: Locally Analytical Numerical Method for Inviscid Oscillating Airfoil Aerodynamics. Presented at the SIAM 1986 National Meeting, Boston, MA, July 1986.
8. Usab, W.J., Jr.; and Verdon, J.M.: On the Application of a Linearized Unsteady Potential Flow Analysis to Fan-Tip Cascades. ASME Paper 86-GT-87, June 1986.
9. Szechenyi, E.; and Girault, J.P.: A Study of Compressor Blade Stall Flutter in a Straight Cascade Wind Tunnel. Aeroelasticity in Turbomachines, P. Suter, ed., Juris-Verlag, 1980, pp. 163-169.
10. Davies, M.R.D.; and Whitehead, D.S.: Unsteady Aerodynamic Moment Measurements in a Transonic Annular Cascade. Unsteady Aerodynamics of Turbomachines and Propellers, D.S. Whitehead, ed., University Press, 1984, pp. 487-502.
11. Shaw, L.M., et al.: Unsteady Pressure Measurements on a Biconvex Airfoil in a Transonic Oscillating Cascade. J. Eng. Gas Turbines Power, vol. 108, no. 1, Jan. 1985, pp. 53-59. (NASA TM-86914).
12. Burgess, J.C.: On Digital Spectrum Analysis of Periodic Signals. J. Acoust. Soc. Am., vol. 58, no. 3, Sept. 1975, pp. 556-567.

13. Carta, F.O.; and Lorber, P.F.: Experimental Study of the Aerodynamics of Incipient Torsional Stall Flutter. J. Propulsion, vol. 3, no. 2, Mar.-Apr. 1987, pp. 164-170.

TABLE I. - AIRFOIL AND CASCADE GEOMETRY

Airfoil	
Type	Biconvex, no camber
Surface radius of curvature, cm	27.4
Leading- and trailing-edge radii of curvature, cm	0.025
Thickness, T, cm	0.58
Chord, C, cm	7.62
Elastic axis	Midchord
Dynamic pressure transducer locations, percent chord	12,25,40 60,75,88
Cascade	
Number of airfoils	9
Solidity, C/S	1.3
Spacing, S, cm	5.86
Stagger angle, q, deg	53
Amplitude of motion, deg	1.2

TABLE II. - EXPERIMENTAL CONDITIONS

Mach number	Mean incidence angle, deg	Interblade phase angle, deg	Reduced frequency
0.65	0	0, 90, -90	0.223, 0.390, 0.557
.65	7	0, 90, -90	0.223, 0.390, 0.557
.80	7	0, 90, -90	0.185, 0.462

TABLE III. - ACOUSTIC RESONANCE CONDITIONS

Mach number	Reduced frequency	Interblade phase angle, deg
0.65	0.223	-8.9, 31.9
	.390	-15.6, 55.8
	.557	-22.2, 79.7
.80	.185	-8.6, 54.9
	.323	-15.1, 96.2
	.462	-21.5, 137.1

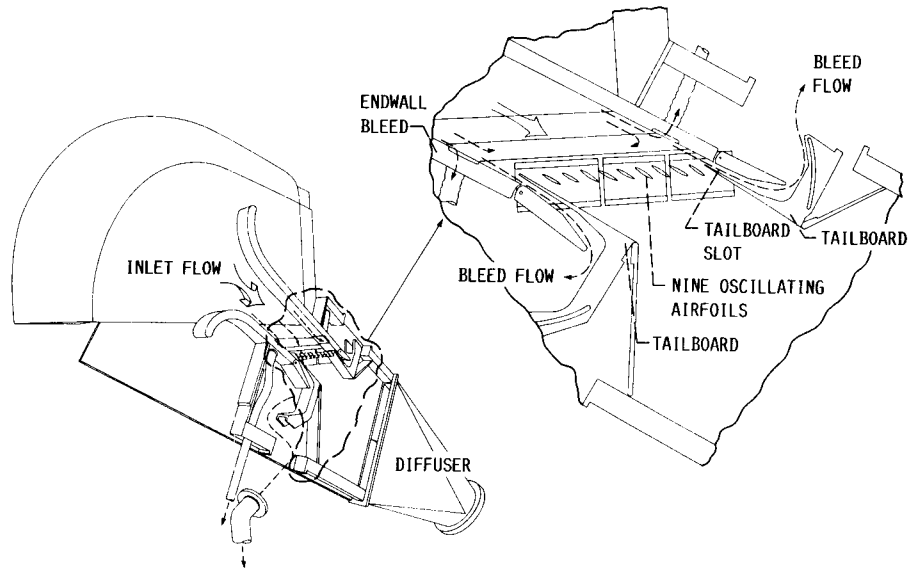


FIGURE 1. - NASA LEWIS TRANSONIC OSCILLATING CASCADE FACILITY.

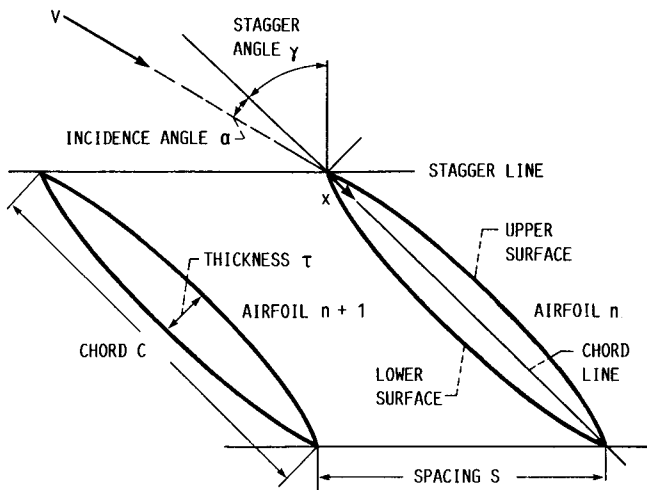


FIGURE 2. - CASCADE GEOMETRY.

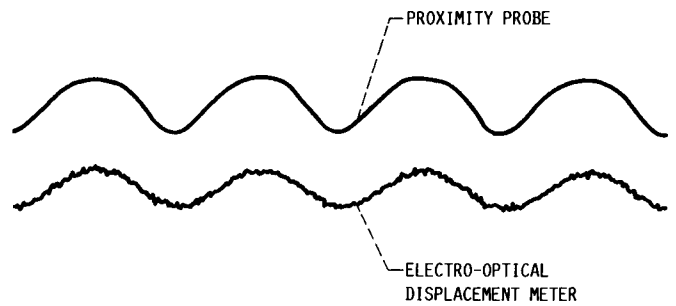


FIGURE 3. - SAMPLE AIRFOIL MOTION SIGNALS.

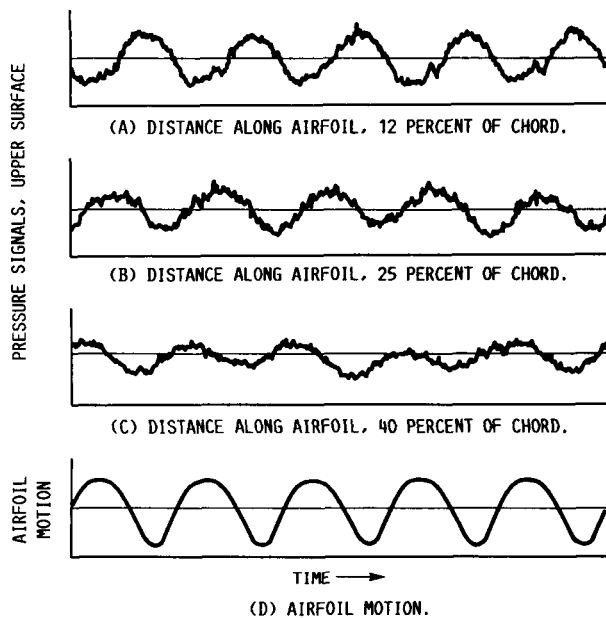


FIGURE 4. - TIME-VARIANT SIGNALS. FREE-STREAM MACH NUMBER, M , 0.80; MEAN FLOW INCIDENCE ANGLE, α_0 , 7° ; INTERBLADE PHASE ANGLE, σ , 90° ; REDUCED FREQUENCY, k , 0.185.

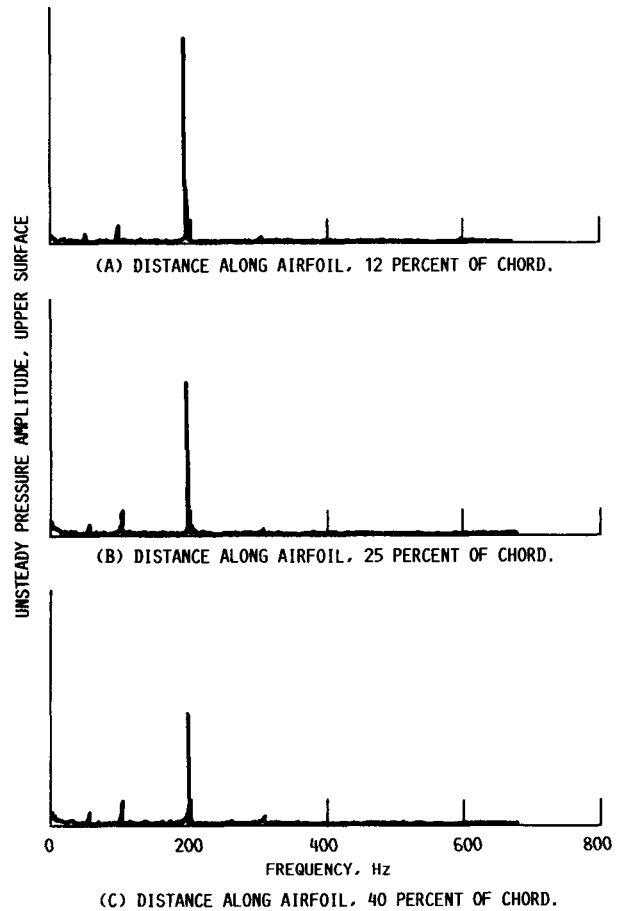


FIGURE 5. - AVERAGED PRESSURE SPECTRA. FREE-STREAM MACH NUMBER, M , 0.80; MEAN FLOW INCIDENCE ANGLE, α_0 , 7° ; INTERBLADE PHASE ANGLE, σ , 90° ; REDUCED FREQUENCY, k , 0.185.

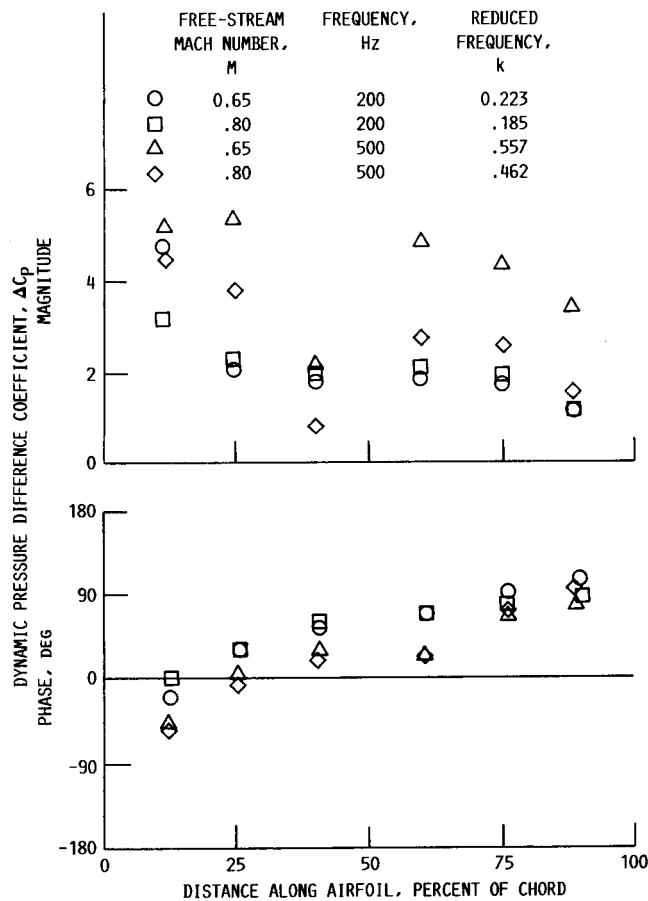


FIGURE 6. - EFFECT OF MACH NUMBER ON DYNAMIC PRESSURE DIFFERENCE COEFFICIENT. MEAN FLOW INCIDENCE ANGLE, α_0 , 7° ; INTERBLADE PHASE ANGLE, σ , 0° .

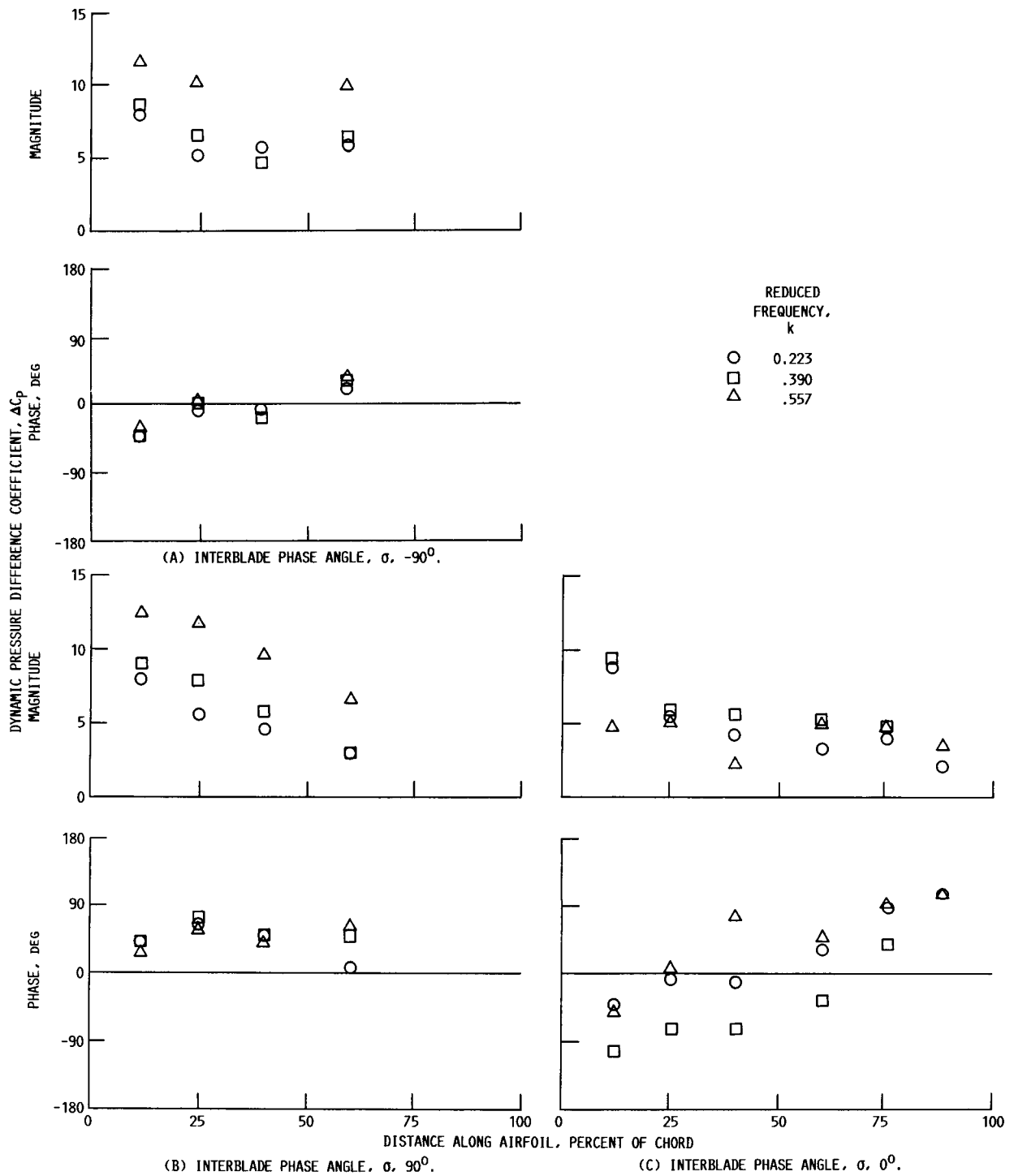


FIGURE 7. - EFFECT OF REDUCED FREQUENCY ON DYNAMIC PRESSURE DIFFERENCE COEFFICIENT AT FREE-STREAM MACH NUMBER M OF 0.65 AND MEAN FLOW INCIDENCE ANGLE α_0 OF 0° .

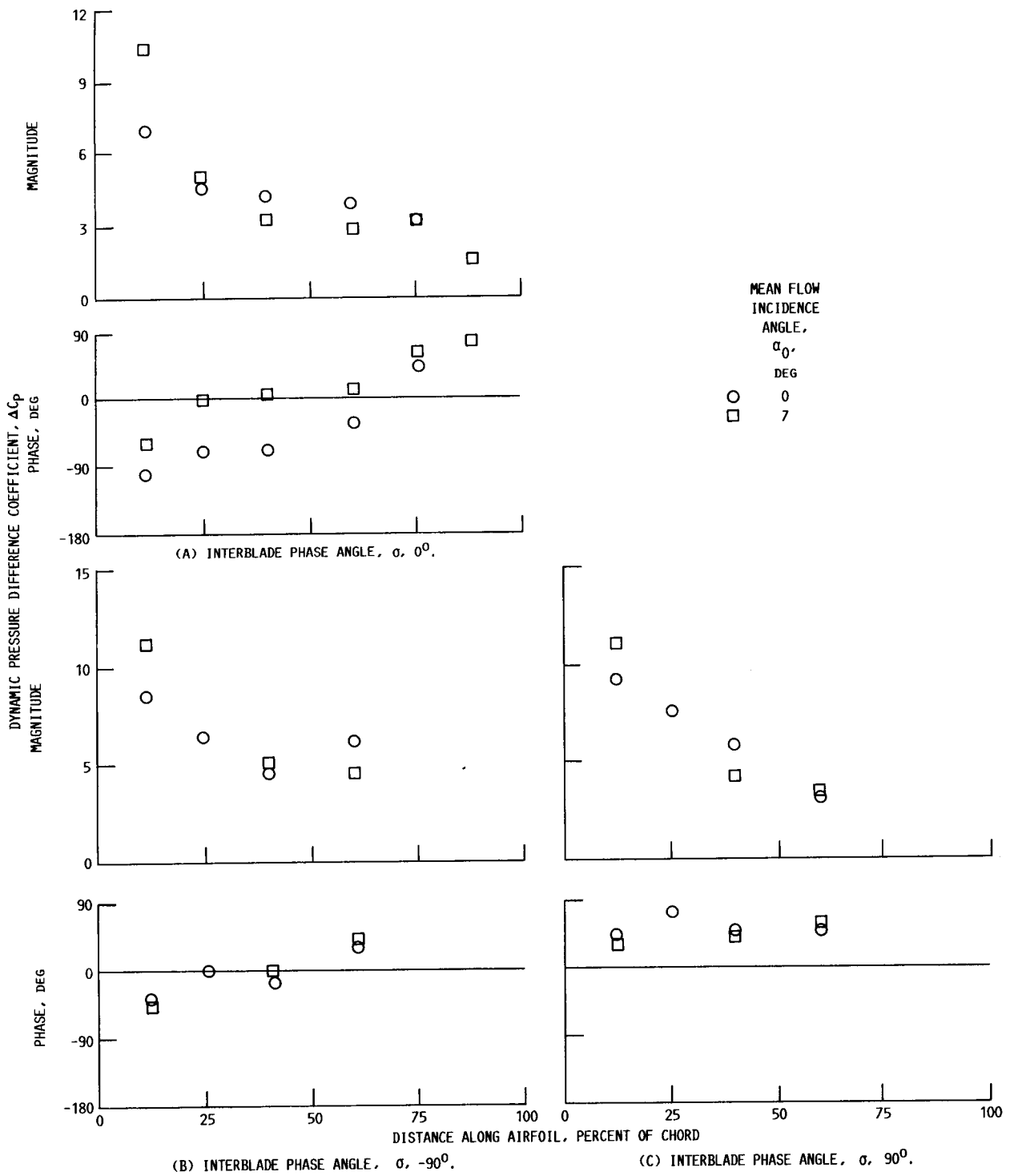


FIGURE 8. - EFFECT OF MEAN FLOW INCIDENCE ON DYNAMIC PRESSURE DIFFERENCE COEFFICIENT AT FREE-STREAM MACH NUMBER M OF 0.65 AND REDUCED FREQUENCY k OF 0.390.

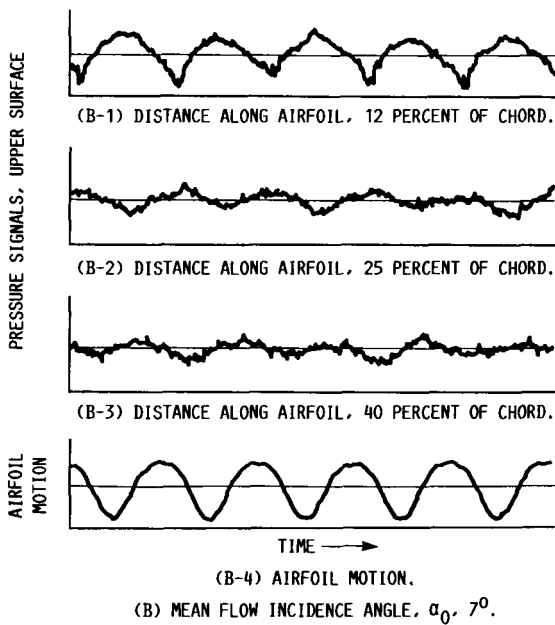
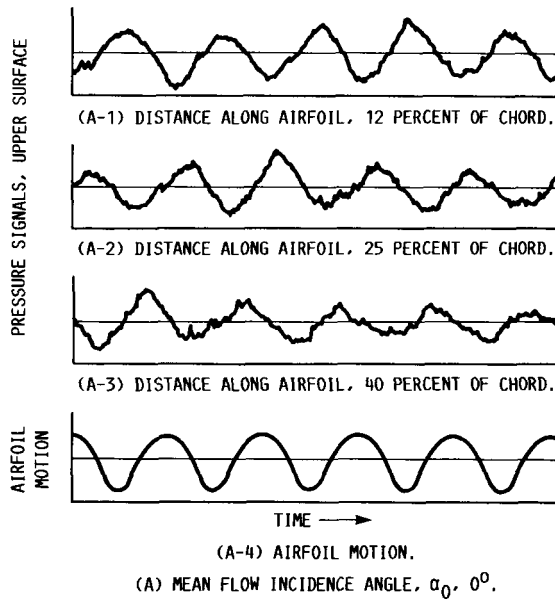


FIGURE 9. - AIRFOIL UPPER SURFACE UNSTEADY SIGNALS
 AT FREE-STREAM MACH NUMBER M OF 0.65, INTER-
 BLADE PHASE ANGLE σ OF 90° , AND REDUCED FREQUENCY
 k OF 0.223.

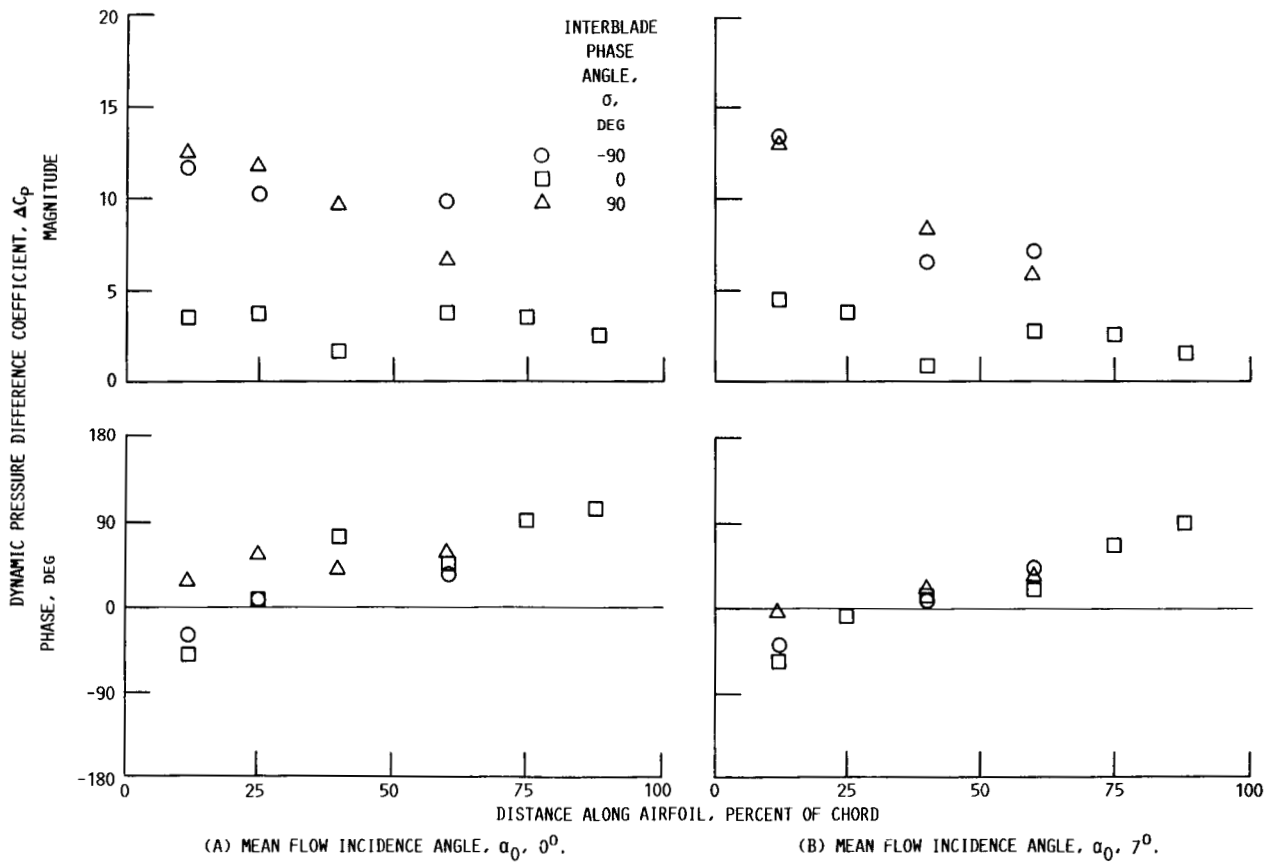
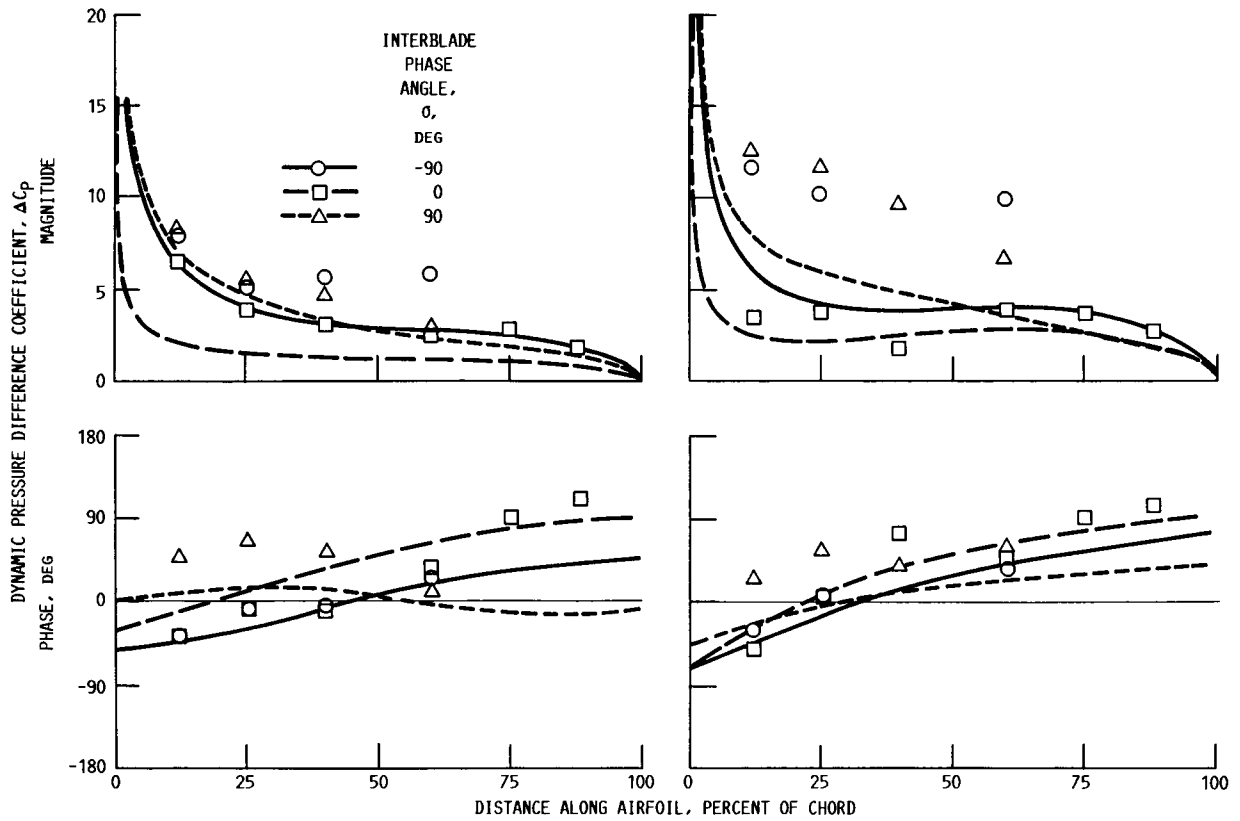


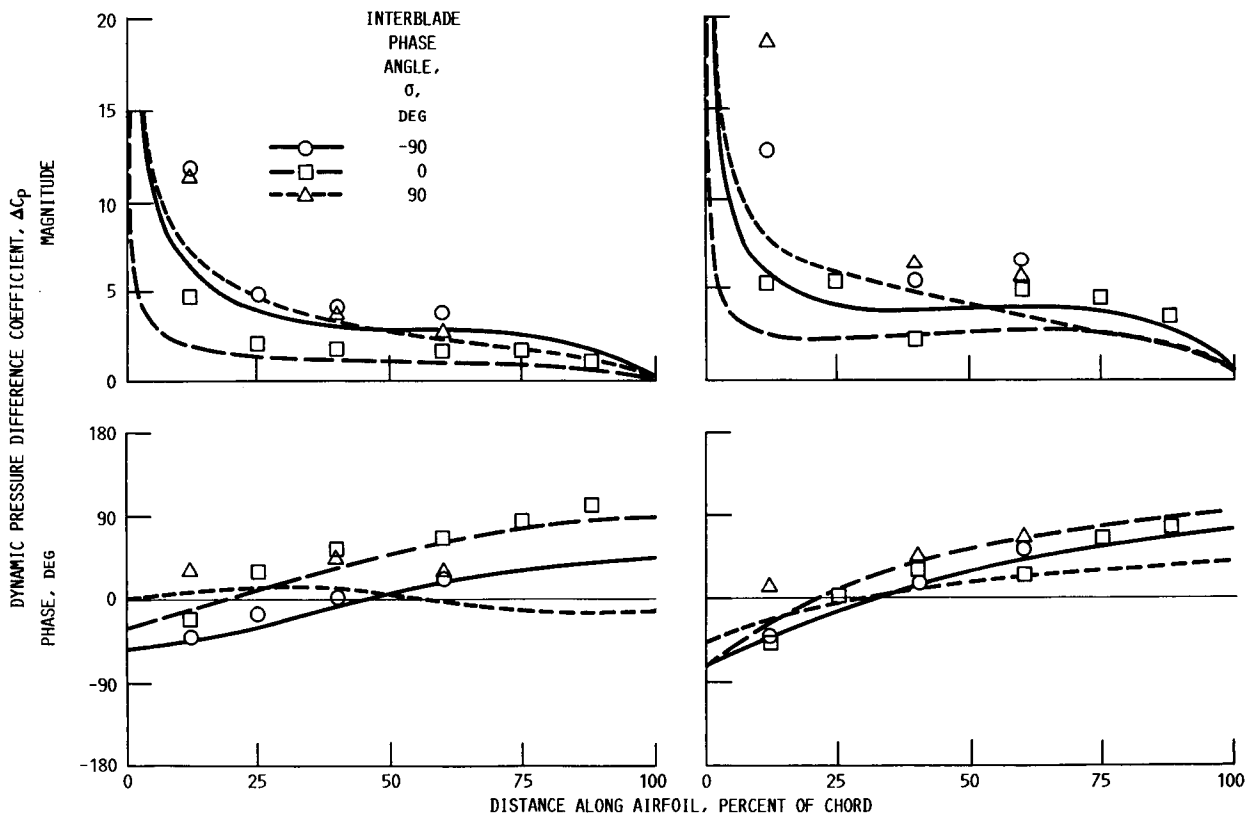
FIGURE 10. - EFFECT OF INTERBLADE PHASE ANGLE ON DYNAMIC PRESSURE DIFFERENCE COEFFICIENT AT FREE-STREAM MACH NUMBER M OF 0.65 AND REDUCED FREQUENCY k OF 0.557.



(A) REDUCED FREQUENCY, 0.223.

(B) REDUCED FREQUENCY, 0.557.

FIGURE 11. - DATA-LINEARIZED THEORY CORRELATION AT FREE-STREAM MACH NUMBER M OF 0.65 AND MEAN FLOW INCIDENCE ANGLE α_0 OF 0° .



(A) REDUCED FREQUENCY, 0.223.

(B) REDUCED FREQUENCY, 0.557.

FIGURE 12. - DATA-LINEARIZED THEORY CORRELATION AT FREE-STREAM MACH NUMBER M OF 0.65 AND MEAN FLOW INCIDENCE ANGLE α_0 OF 7° .

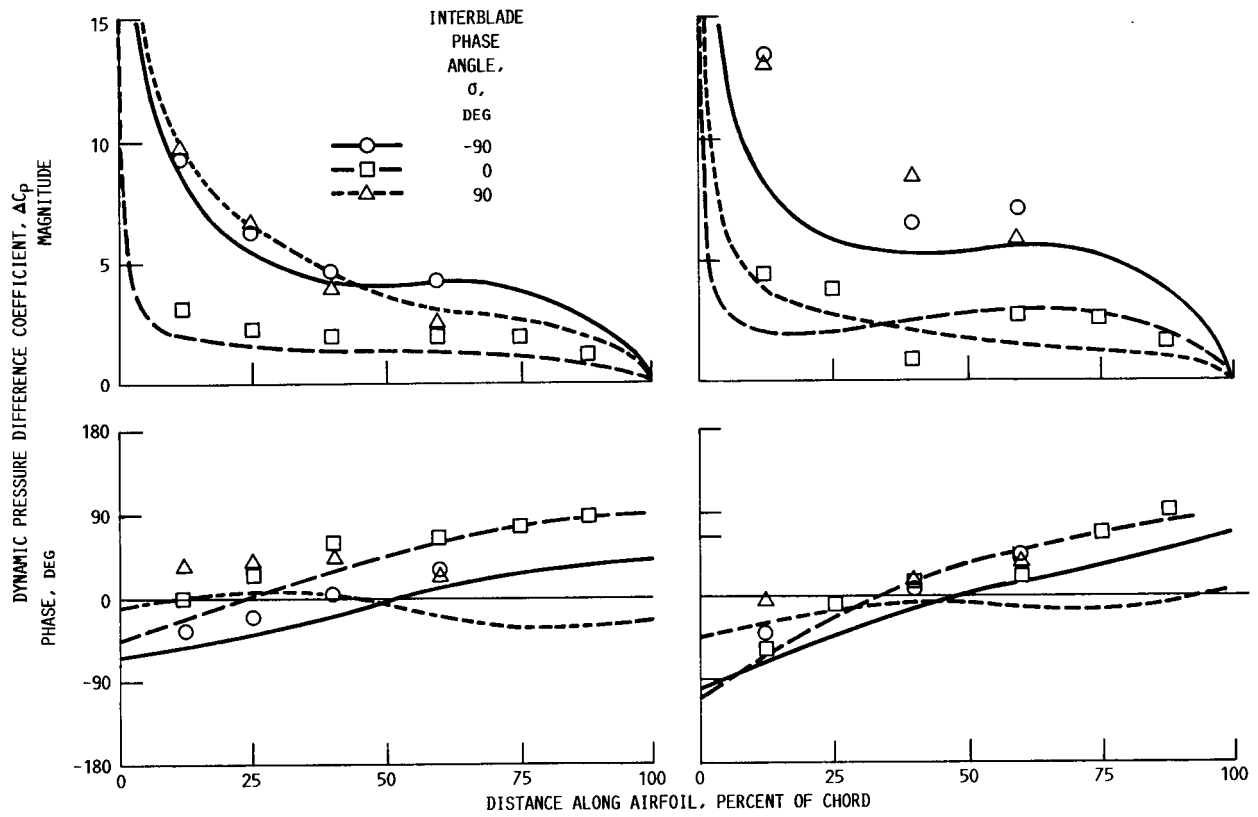


FIGURE 13. - DATA-LINEARIZED THEORY CORRELATION AT FREE-STREAM MACH NUMBER M OF 0.80 AND MEAN FLOW INCIDENCE ANGLE α_0 OF 7° .

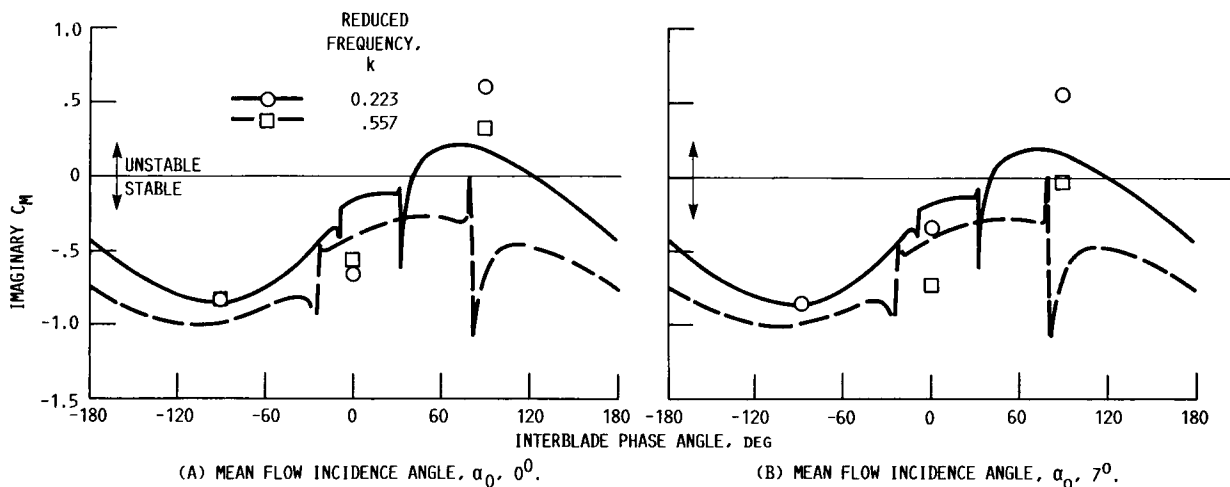


FIGURE 14. - IMAGINARY MOMENT COEFFICIENT VARIATION WITH INTERBLADE PHASE ANGLE AT FREE-STREAM MACH NUMBER M OF 0.65.

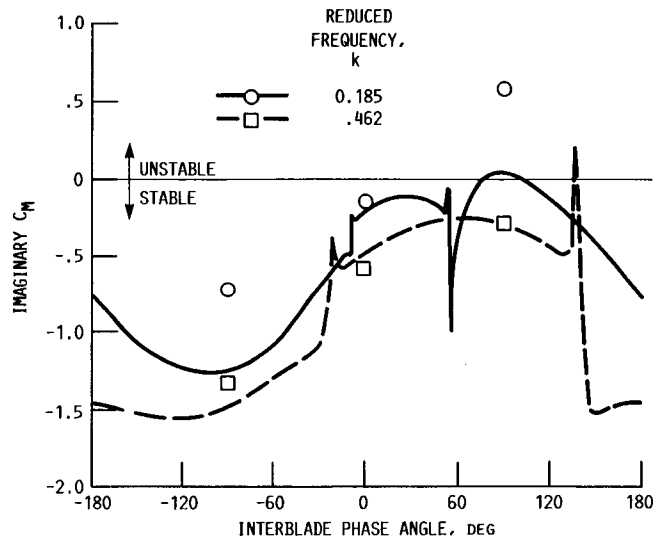


FIGURE 15. - IMAGINARY MOMENT COEFFICIENT VARIATION WITH INTERBLADE PHASE ANGLE AT FREE-STREAM MACH NUMBER M OF 0.80 AND MEAN FLOW INCIDENCE ANGLE α_0 OF 7° .



Report Documentation Page

1. Report No. NASA TM-100219	2. Government Accession No.	3. Recipient's Catalog No.	
4. Title and Subtitle Unsteady Aerodynamics of an Oscillating Cascade in a Compressible Flow Field		5. Report Date	
		6. Performing Organization Code	
7. Author(s) Daniel H. Buffum, Donald R. Boldman, and Sanford Fleeter		8. Performing Organization Report No. E-3830	
		10. Work Unit No. 535-03-01	
9. Performing Organization Name and Address National Aeronautics and Space Administration Lewis Research Center Cleveland, Ohio 44135-3191		11. Contract or Grant No.	
		13. Type of Report and Period Covered Technical Memorandum	
12. Sponsoring Agency Name and Address National Aeronautics and Space Administration Washington, D.C. 20546-0001		14. Sponsoring Agency Code	
		15. Supplementary Notes Prepared for the 4th Symposium on Unsteady Aerodynamics and Aeroelasticity of Turbomachines and Propellers sponsored by Aachen University of Technology, Aachen, West Germany, September 6-10, 1987. Daniel H. Buffum and Donald R. Boldman, NASA Lewis Research Center; Sanford Fleeter, Thermal Sciences and Propulsion Center, School of Mechanical Engineering, Purdue University, West Lafayette, Indiana 47907.	
16. Abstract <p>Fundamental experiments were performed in the NASA Lewis Transonic Oscillating Cascade Facility to investigate and quantify the unsteady aerodynamics of a cascade of biconvex airfoils executing torsion-mode oscillations at realistic reduced frequencies. Flush-mounted, high-response miniature pressure transducers were used to measure the unsteady airfoil surface pressures. The pressures were measured for three interblade phase angles at two inlet Mach numbers, 0.65 and 0.80, and two incidence angles, 0° and 7°. The time-variant pressures were analyzed by means of discrete Fourier transform techniques, and these unique data were then compared with predictions from a linearized unsteady cascade model. The experimental results indicate that the interblade phase angle had a major effect on the chordwise distributions of the airfoil surface unsteady pressure, and that reduced frequency, incidence angle, and Mach number had a somewhat less significant effect.</p>			
17. Key Words (Suggested by Author(s)) Unsteady aerodynamics Cascade flow Flutter		18. Distribution Statement Unclassified - Unlimited Subject Category 07	
19. Security Classif. (of this report) Unclassified	20. Security Classif. (of this page) Unclassified	21. No of pages 20	22. Price* A02